



Network dynamics of the brain and influence of the epileptic seizure onset zone

Samuel P. Burns^{a,1}, Sabato Santaniello^{a,1,2,3}, Robert B. Yaffe^{a,b}, Christophe C. Jouny^c, Nathan E. Crone^c, Gregory K. Bergey^c, William S. Anderson^{a,d}, and Sridevi V. Sarma^{a,b,3}

^aInstitute for Computational Medicine and ^bDepartment of Biomedical Engineering, The Johns Hopkins University, Baltimore, MD 21218; and ^cEpilepsy Center, Department of Neurology, and ^dDepartment of Neurosurgery, The Johns Hopkins School of Medicine, Baltimore, MD 21287

Edited by Nicholas R. Anderson, Novel Research Associates, Fairfield, CA, and accepted by the Editorial Board October 7, 2014 (received for review February 5, 2014)

The human brain is a dynamic networked system. Patients with partial epileptic seizures have focal regions that periodically diverge from normal brain network dynamics during seizures. We studied the evolution of brain connectivity before, during, and after seizures with graph-theoretic techniques on continuous electrocorticographic (ECoG) recordings (5.4 ± 1.7 d per patient, mean \pm SD) from 12 patients with temporal, occipital, or frontal lobe partial onset seizures. Each electrode was considered a node in a graph, and edges between pairs of nodes were weighted by their coherence within a frequency band. The leading eigenvector of the connectivity matrix, which captures network structure, was tracked over time and clustered to uncover a finite set of brain network states. Across patients, we found that (i) the network connectivity is structured and defines a finite set of brain states, (ii) seizures are characterized by a consistent sequence of states, (iii) a subset of nodes is isolated from the network at seizure onset and becomes more connected with the network toward seizure termination, and (iv) the isolated nodes may identify the seizure onset zone with high specificity and sensitivity. To localize a seizure, clinicians visually inspect seizures recorded from multiple intracranial electrode contacts, a time-consuming process that may not always result in definitive localization. We show that network metrics computed from all ECoG channels capture the dynamics of the seizure onset zone as it diverges from normal overall network structure. This suggests that a state space model can be used to help localize the seizure onset zone in ECoG recordings.

focal epilepsy | seizure localization | network analysis | eigenvector centrality | ECoG signals

Epilepsy affects over 60 million people worldwide, and approximately 40% of patients have drug-resistant epilepsy (DRE) with recurrent seizures that are not controlled by available medications (1–3). It is now routine to consider drug-resistant partial epilepsy patients, who represent the largest cohort of patients with uncontrolled seizures, for possible resective seizure surgery (4). Successful seizure surgery is predicated upon the ability to localize the seizure onset zone. Although some patients (e.g., those with mesial temporal sclerosis or lesional epilepsy) can proceed to surgery following scalp recordings of seizures delineating a seizure onset zone (5), a significant number of patients have seizures that are challenging to localize with scalp ictal (i.e., seizure) recordings. In this case, ictal recordings using intracranial electrodes (e.g., subdural strips, grids, or depth electrode arrays) are necessary. The purpose of these intracranial recording arrays is to provide information about seizure onset and propagation, representing spatiotemporal changes in cerebral function.

Using intracranial electrocorticographic (ECoG) recordings taken over several days to capture ictal events, clinicians visually inspect the ECoG recordings at the onset of the seizures and look for signatures on individual channels (e.g., rhythmic spiking, low-voltage fast activity, etc.) that might be characteristic of the seizure onset zone (6). With the large numbers of implanted electrodes (typically more than 100 contacts), this can be time-

consuming even for epileptologists who are quick and experienced. Moreover, the activity on individual channels is affected by functional networks that may involve many channels in the surrounding regions, and this is not always easily detected through visual inspection. Hence, seizure onset zone localization can be challenging in a significant number of patients (e.g., nonlesional) (7, 8).

In particular, it is unknown whether or not a consistent structure emerges over time in brain functional networks during interictal and ictal periods. To date, brain connectivity has been studied by using intracranial ECoG recordings from brief temporal intervals only (tens to a few hundreds of seconds) in either interictal periods or ictal periods (9–19), or neuronal ensembles have been studied *in vitro* (20–22). Only a handful of studies have examined the role of the clinically annotated focus (i.e., the region that is clinically identified as the seizure onset zone and subsequently surgically resected) in brain networks over time (23–28).

To further investigate the spatiotemporal mechanisms of cerebral function and to investigate whether a consistent structure emerges over time in brain functional networks, we used a network-based analysis and ECoG recordings from subdural and depth electrodes in 12 patients with DRE undergoing presurgical evaluations. We measured brain connectivity continuously (i.e., every second) during interictal, periictal, and ictal periods spanning several days (5.4 ± 1.7 d per patient, mean \pm SD), and, for each patient, we used unsupervised clustering to group all of the networks computed over time into a finite set of distinct networks.

Significance

In epilepsy, seizures elicit changes in the functional connectivity of the brain that shed insight into the seizures' nature and onset zone. We investigated the brain connectivity of patients with partial epileptic seizures from continuous multiday recordings and found that (i) the connectivity defines a finite set of brain states, (ii) seizures are characterized by a consistent progression of states, and (iii) the seizure onset zone is isolated from the surrounding regions at seizure onset but becomes most connected toward seizure termination. Our results suggest that a finite-dimensional state space model may characterize the dynamics of the epileptic brain and ultimately help localize the seizure onset zone, which is currently done by clinicians through visual inspection of electrocorticographic recordings.

Author contributions: S.P.B., N.E.C., G.K.B., W.S.A., and S.V.S. designed research; S.P.B., R.B.Y., C.C.J., W.S.A., and S.V.S. performed research; S.P.B., S.S., and R.B.Y. analyzed data; and S.P.B., S.S., N.E.C., G.K.B., W.S.A., and S.V.S. wrote the paper.

The authors declare no conflict of interest.

This article is a PNAS Direct Submission. N.R.A. is a guest editor invited by the Editorial Board.

¹S.P.B. and S.S. contributed equally to this work.

²Present address: Department of Biomedical Engineering, University of Connecticut, Storrs, CT 06269.

³To whom correspondence may be addressed. Email: ssarma2@jhu.edu or sabato@engr.uconn.edu.

Finally, if a robust set of clusters emerged, we examined how the brain transitions between these network clusters (brain states).

Across all patients, we found that the interictal activity enters only a small set of distinct states (two to five), whereas there are 2–11 states during seizures. We also found that, during seizures, the brain transitions through a finite set of network states in a reproducible manner, i.e., the pattern is the same across different seizures in the same patient, with characteristic onset and termination. These findings suggest that the brain connectivity may be described in a low-dimensional state space.

Moreover, the uncovered brain states allowed us to characterize the activity in the seizure onset zone before, during, and after ictal events, which may help understand the role of the zone in network connectivity dynamics. In particular, for each brain state revealed by our analysis, we studied the connectivity of the clinically annotated seizure onset zone to the remaining brain network and we found that there is a specific state during seizures that consistently occurs shortly after the seizure begins (especially in patients with successful surgeries that likely had adequate electrode coverage of the seizure onset zone). In this state, the seizure onset zone is significantly isolated from the rest of the network.

In *Discussion*, we describe how the isolated state of the seizure onset zone may be used to assist in the development of a method to localize the seizure onset zone from intracranial ECoG recordings. Characterization and localization of the seizure onset zone are of utmost importance to guide subsequent surgical resection, which is still the best therapeutic alternative for patients with DRE (4). However, failure to optimally identify the seizure onset zone can occur even with intracranial ECoG recordings, particularly in patients with nonlesional epilepsy, and this can result in suboptimal surgical outcomes and a high chance (~40%) of seizure recurrence within one year postsurgery (7, 8). Preliminary results of this study were presented in (29).

Results

We analyzed the functional brain connectivity across 42 seizures in 12 DRE patients with temporal, occipital, or frontal lobe partial seizures over several days of continuous multichannel intracranial ECoG recordings (average values per patient: 130.7 ± 40.9 h of ECoG recordings, 88 ± 22 electrodes, 3.5 ± 1.51 seizures; mean \pm SD). See details in Tables 1 and 2. We studied the pattern of network connectivity over time, and we assessed the centrality

of the clinically assigned seizure onset zone to the dominant connectivity during seizures.

Network Analysis. For each patient, we tracked the evolution of the brain network over consecutive windows (window length: 2.5 s; overlap: 1.5 s) by computing a connectivity matrix from the multielectrode ECoG data in each window, which resulted in one matrix per 1 s of data segment.

Each electrode was considered a node in a graph, and edges were weighted by the average normalized coherence in a fixed frequency band (see definition in *Materials and Methods*). This band varied with the patient and was one among [1, 4] Hz, [5, 8] Hz (theta), [9, 13] Hz (alpha), [14, 25] Hz (beta), [25, 90] Hz (gamma), and [100, 200] Hz (Table 2). For each patient, the band was determined by computing the average r-spectrum across all of the ECoG electrodes and choosing the frequency window with the greatest modulation during seizure (Fig. 1).

The resultant connectivity matrices revealed a consistent pattern around seizures. Fig. 2 shows ECoG recordings from 10 focal electrodes in a patient (Fig. 2A) and three samples of connectivity matrices computed at the electrographic onset time of the seizure, 100 s after onset, and 200 s after onset, respectively (Fig. 2B). The connectivity was weakest at the electrographic onset time (left plot). Then, after 100 s, channels in the temporal lobe (central plot: channels 5–22, 45–47, 52–54, 58–65, 80–86) developed into a connected subnetwork and gradually grew until most electrodes were strongly connected 200 s after the onset (right plot).

The network connectivity at each second was summarized by computing the eigenvector centrality (EVC) of the nodes from the correspondent connectivity matrix, where the EVC captures the importance of each electrode (node) in the graph (30). For the case in Fig. 2, the EVCs (Fig. 2C) capture the pattern of weak connectivity at the electrographic onset time, increase at 100 s, and finally indicate, at 200 s, that most electrodes have nearly equal (high) centrality, which suggests that most electrodes in the network are strongly connected to one another.

Brain States. The EVCs can be represented as vectors in the \mathbb{R}^N space, where N is the number of electrodes (30). As the EVCs change in time, the corresponding vectors point in different directions in \mathbb{R}^N , and we used the directions (subspaces) visited by the EVCs under different conditions to define the brain states.

Table 1. Patients with drug-resistant epilepsy

ID	Age/sex	Type	SZ type	Elc.	Surgery	Outcome
Group 1						
1	18/M	Lesional, temporal	CPS+GTC	S	Left anterior TL, AMG, and partial HIPP	Seizure recurrence
2	17/F	Lesional, extratemporal	CPS+GTC	S	Right inferior OL	Seizure free
3	14/na	Lesional, extratemporal	CPS+GTC	S	Left posterior PL	Seizure free
Group 2						
4	49/F	Lesional, temporal	CPS	S	Left selective AMG and HIPP	Seizure free
5	5/M	Nonlesional, extratemporal	PS	S	Right posterior TL and OL	Seizure free
6	24/M	Lesional, extratemporal	CPS	S	Right anterior TL, AMG, and HIPP, and frontal PL	Seizure free
7	36/M	Lesional, extratemporal	PS	S + D	Right FL, right PL	Seizure free
8	24/M	na	PS	S + D	Right OL, right PL	Seizure free
Group 3						
9	34/M	Nonlesional, temporal	CPS	S	Left TL	Seizure recurrence
10	29/F	Lesional, extratemporal	CPS	S	Right TL, partial OL	Seizure recurrence
11	24/M	Nonlesional, extratemporal	CPS	S + D	Left FL	Seizure recurrence
12	31/M	Nonlesional, extratemporal	CPS	S + D	Left FL	Seizure recurrence

Groups 1 and 2 include patients who had a single resection. Group 3 includes patients that had previous resection surgeries. AMG, amygdalectomy; CPS, complex partial seizure; D, depth electrodes; Elc., electrode type; FL, frontal lobectomy; GTC, secondarily generalized tonic-clonic seizure; HIPP, hippocampectomy; na, information not available; OL, occipital lobectomy; PL, parietal lobectomy; PS, simple partial seizure; S, subdural grid electrodes; “Seizure free” means that no seizure was reported within six months; “Seizure recurrence” means that seizures recurred within six months postsurgery; SZ, seizure; TL, temporal lobectomy.

Table 2. ECoG recordings and results

ID	S/D	Time	No. seizures	r-spectrum peak band	No. states (II, Pre, SZ, Post)	Earliest max ROC AUC IF/time	Earliest max ROC AUC CF/time	P value state transitions
Group 1								
1	75/0	132.1	3	Beta	(3, 3, 6, 2)	0.93/0.17	0.83/0.55	<0.0001
2	40/0	113.4	2	Beta	(2, 2, 5, 2)	0.77/0.0	0.74/0.41	0.25
3	94/0	131.7	4	Alpha	(2, 4, 11, 1)	0.91/0.14	0.76/0.94	0.0006
Group 2								
4	82/0	137.4	4	Beta	(3, 3, 4, 5)	0.85/0.0	0.41/0.21	<0.0001
5	79/0	45.9	5	Beta	(2, 2, 3, 2)	0.87/0.28	0.73/0.99	0.041
6	65/2	231.4	2	Beta	(3, 2, 2, 2)	0.87/0.0	0.61/0.13	0.55
7	99/4	129.5	2	Theta	(2, 2, 3, 3)	0.84/0.24	0.46/0.01	0.62
8	101/3	137.7	7	Beta	(5, 3, 4, 4)	0.50/0.99	0.60/0.04	0.83
Group 3								
9	89/0	106.3	4	Beta	(3, 3, 6, 2)	0.54/0.84	0.66/0.39	0.0013
10	110/0	140.1	3	Beta	(2, 5, 3, 3)	0.43/0.39	0.63/0.01	0.84
11	116/3	132.2	4	Gamma	(3, 1, 3, 1)	0.56/0.69	0.47/0.11	0.0004
12	112/2	131.5	2	Gamma	(2, 3, 2, 2)	0.56/0.0	0.54/0.29	0.084

Number of electrodes, seizures, and brain states, and results of the ROC analysis. II, interictal; Post, postictal epoch; Pre, preictal epoch; S/D, number of subdural (S) and depth (D) electrodes; SZ, seizure; "Time" denotes the duration (in hours) of the continuous recordings per patient. The numbers under the column labeled "No. states" indicate the number of brain states uncovered during each period II, Pre, SZ, and Post. The "Earliest max ROC AUC IF/time" is the maximum area under the ROC curve achieved when using the centroid vector obtained in the IF state near the beginning of seizure. The "Earliest max ROC AUC CF/time" is the maximum area under the ROC curve achieved when using the centroid vector obtained in the CF state near the middle-to-end of seizure.

Specifically, when the EVC vector pointed in the same direction in \mathbb{R}^N over a period of time, the brain was considered to be in a consistent state. When the EVC vector rotated to a new direction, the brain was considered transitioning into a new state.

We analyzed the EVCs for state changes in each patient separately by using unsupervised clustering techniques (31, 32) (*Materials and Methods*). Figs. 3 and 4 report the brain states derived from our analysis for patients 1 and 4 in Tables 1 and 2, respectively.

Patient 1 (complex partial seizures with secondary tonic-clonic generalization) had a r-spectrum peaking in the beta band and the resected focus was located in the temporal lobe near electrodes 67–68, 72–73, and 77–79 (Fig. 3 E and F). A comparison between the spectrograms of interictal and ictal periods (Fig. 3 C and D) shows the occurrence of enhanced activity in the low-frequency range during seizures, which did not appear during interictal periods. Correspondingly, a few patterns in the electrodes' EVCs emerged and abrupt changes between patterns were noted as each seizure progresses (Fig. 3 F). These patterns correspond to specific evolutions of the brain state (Fig. 3 G and

H), were patient specific, and resulted consistent across multiple seizures. Consistency was assessed by using a simulation-based shuffle analysis with significance level $P < 0.05$ (*P value*) (*Materials and Methods*).

In patient 1, all of the seizures reliably progressed through the same set of states (sequence of states: 4 → 6 → 8 → 7 → 5 → 6), and eventually visited state 9 late in seizure, but before the seizure's termination (two out of three seizures). This state transition topology is shown in Fig. 5A. Also, in contrast to the highly variable connectivity during seizures, the connectivity during interictal periods and in 10-minute-long windows right before and after seizure (preictal and postictal epochs, respectively) was relatively stable (Fig. 3 E and F), with the brain visiting a smaller number of states (Fig. 3 G and H).

Fig. 4 illustrates our analysis for a complex partial seizure without secondary generalization recorded from patient 4. The r-spectrum peaked in the beta band and the resected focus was located in the occipital lobe near electrodes 41 and 46. A characteristic spectrogram modulation was reported during seizure (Fig. 4 C and D), and, correspondingly, discrete state changes in the EVCs emerged (Fig. 4 F), even though they were not visually apparent in the ECoG time series (Fig. 4 B–D). In this patient, the progression of state changes across all of the seizures showed a consistent structure (sequence of states: 4 → 6 → 7 → 5 → 7; Fig. 4 G and H), with significant differences from the case with tonic-clonic secondary generalization (e.g., the seizures here oscillated between states 5 and 7 and revisited state 4, which occurred right at the beginning of the seizure, before suppression; Fig. 5B).

In both patients, there were fewer interictal states (three states only) and the intrastate distances between interictal states (i.e., difference between the correspondent EVC vectors) were smaller than the intrastate distances estimated during the ictal periods and the pre/postictal epochs. Moreover, differently from the patterned evolution of the states during seizures, the state changes during interictal periods did not follow a regular progression. Table 2 reports results for the remaining patients.

Relationship Between Brain States and Seizure Onset Zone. Once the brain states were determined for each patient, we examined the role of the clinically assigned seizure onset zone in each state. All of the electrodes located within the resected region (Table 1)

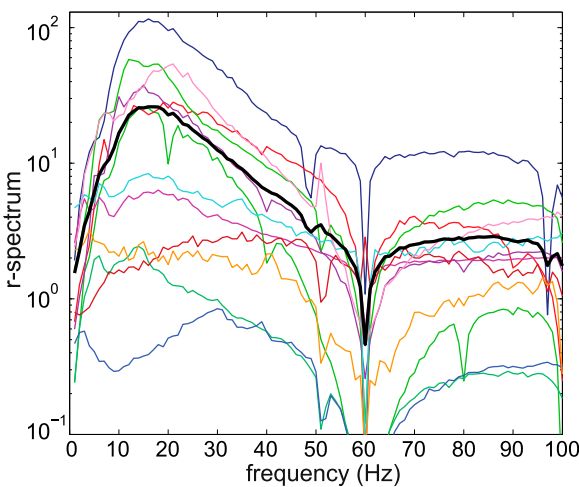


Fig. 1. Population-averaged r-spectrum (black curve) and mean r-spectrum for each patient (nonblack curves).

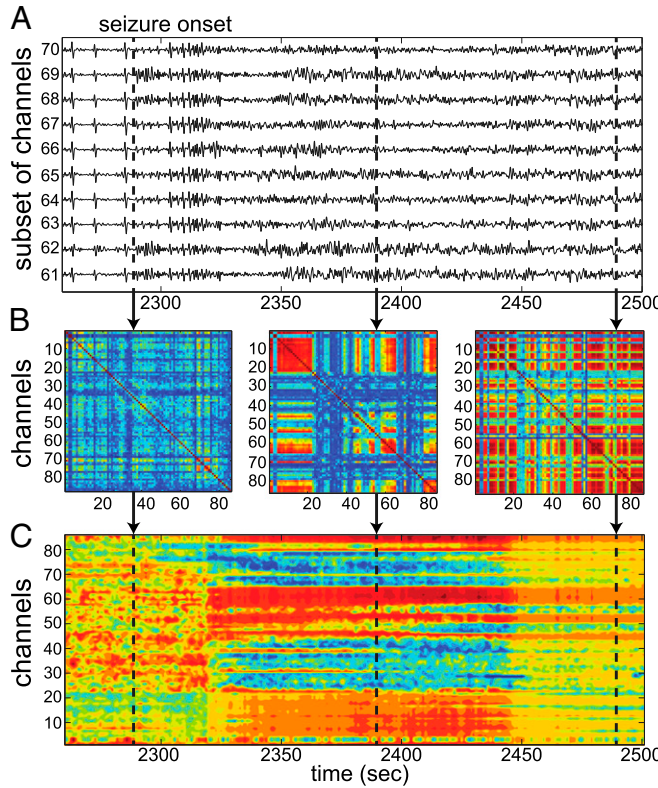


Fig. 2. (A) ECoG recordings from the seizure onset zone as the seizure begins. (B) Rescaled standardized connectivity matrices (C) computed at the times marked by the vertical dashed lines. The matrices show an increase in connectivity between the electrodes as the seizure progresses. (C) Eigenvector centralities (EVCs) computed from the matrices in B. EVCs indicate a change in the topology of brain connectivity between the three vertically marked time periods. The most central electrodes to the connectivity are in red, and the most isolated ones are in blue.

were assumed to record from the focal area. This assumption is reasonable for patients with successful surgical outcomes (patients 2–8, Table 1), but may not hold in patients with failed surgeries (e.g., patients 9–12, Table 1).

We found that, in patients with positive surgical outcomes (i.e., patients who were seizure-free after surgery; Table 1), the focal areas were the least connected in the network (least important) shortly after the onset time of the seizure and we denoted this state as the “isolated focus” (IF) state. We also found that, in many of these patients, the focal areas became most connected in the network in a brain state that occurred during the middle or end of the seizures, and we defined this state as the “connected focus” (CF) state. The network structures that define these states are shown superimposed on standard brain images in Fig. 5 A and B for patients in Figs. 3 and 4, respectively. In these figures, the red nodes denote the clinically assigned seizure onset zone and the blue ones denote the remaining electrodes. The diameter of each node is proportional to the correspondent EVC, and the edge weights are derived from the state’s centroid connectivity matrix. For patient 1, states 6 and 7 are the IF and CF states, respectively; for patient 4, state 6 is the IF state, but no CF state exists.

Determination of the Seizure Onset Zone Using the IF State. Because an IF state emerged in patients with successful surgeries, we hypothesized that this connectivity pattern might provide a signature of the focal area. We investigated this hypothesis by performing

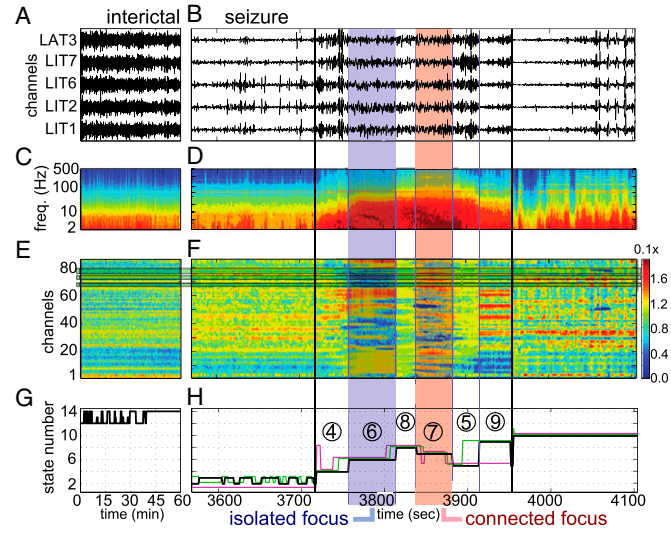


Fig. 3. A patient with secondarily generalized seizures (patient 1). (A and B) ECoG recordings from focal electrodes during an interictal period (A) and a periictal period (B). The period in B includes one seizure, 2.5 min before it (preictal), and 2.5 min after it (postictal). Black vertical lines show seizure onset and termination. (C and D) Power spectrogram averaged across electrodes for the data in A (C) and B (D), respectively. (E and F) Eigenvector centralities (EVCs) of the electrodes during the period in A (E) and B (F), respectively. (G and H) Black lines indicate the states fitted to the EVCs in E (G) and F (H), respectively. In H, the vertical blue lines indicate the state transitions that correspond to the data in B, D, and F, respectively; the non-black horizontal lines indicate the states fitted to the remaining seizures from this patient, scaled to the length of the seizure in B. IF state and CF state are in the blue box and red box, respectively.

a receiver operator characteristic (ROC) analysis on the centroids of the ictal states (31). See details in *Materials and Methods*.

For each patient and identified seizure state, we constructed a resection indicator (RI) vector, i.e., a vector whose entries were 1 for electrodes that corresponded to the seizure onset zone and 0 otherwise, and we compared the state centroid vector to the RI vector in two ways:

- i) IF analysis: We assumed that the least central nodes were indicative of the seizure onset zone; hence, any centroid EVC below a threshold value would be identified as seizure onset zone. For each ictal state, we constructed the ROC curve by varying the threshold and used the area under the ROC curve (AUC) as a measure of performance (33);
- ii) CF analysis: We assumed that the most central nodes were indicative of the seizure onset zone, and therefore any centroid EVC above a threshold value would be identified as seizure onset zone. For each ictal state, we constructed the ROC and measured the AUC values as above.

Figs. 6 and 7 report the results for the patients in Figs. 3 and 4, respectively. Fig. 6A shows the AUC values for states during seizure in case of IF analysis. The centroid that best predicts the resected region occurs approximately 75 s after the onset time of the seizure in all of the seizures and corresponds to state 6 in Fig. 3H. Correspondingly, the AUC value was 0.9 compared with the RI vector, thus indicating a strong relationship. Similarly, the CF analysis (Fig. 6B) indicates that the resected zone is the most connected about 140 s after the seizure onset time in all of the seizures ($AUC > 0.85$). Fig. 6 also shows the centroids associated with the IF and CF state (Fig. 6 C and D), respectively, the normalized connectivity matrices (Fig. 6 E and F), and an image of the left inferior hemisphere of the brain showing the location of the electrodes (Fig. 6G).

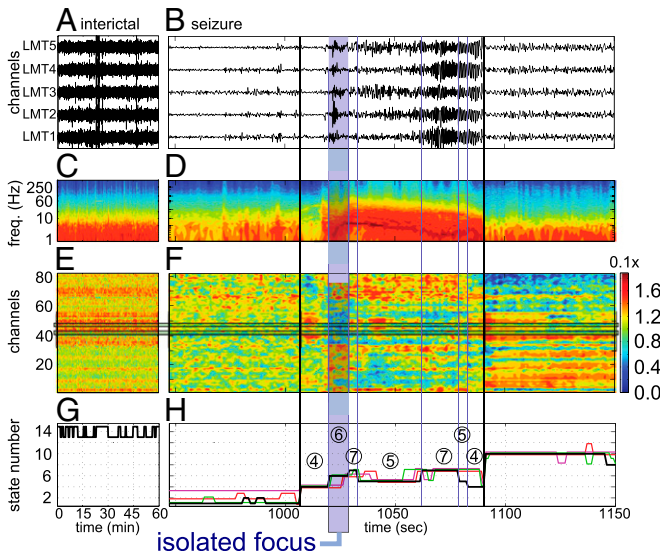


Fig. 4. A patient with complex partial seizures (patient 4). (A and B) ECoG recordings from focal electrodes during an interictal period (A) and a periictal period (B). The period in B includes one seizure, 2.5 min preictal, and 2.5 min postictal. Black vertical lines indicate seizure onset and termination. (C and D) Power spectrogram averaged across electrodes for the data in A (C) and B (D), respectively. (E and F) EVCs of the electrodes during the period in A (E) and B (F), respectively. (G and H) Black lines indicate the states fitted to the EVCs in E (G) and F (H), respectively. In H, the vertical blue lines indicate the state transitions that correspond to the data in B, D, and F, respectively; the nonblack horizontal lines indicate the states fitted to the remaining seizures from this patient, scaled to the length of the seizure in B. The IF state is in the blue box.

In particular, in the matrix associated with the IF state (Fig. 6E), the resected regions are either disconnected from the rest of the brain network (LIT electrodes, Fig. 6G) or only weakly connected (LAT electrodes, Fig. 6G). In contrast, the matrix associated with the CF state (Fig. 6F) shows that both LIT and LAT electrodes are highly connected in this state (i.e., the seizure onset zone is strongly connected locally within the temporal lobe) but also that the seizure onset zone has strong connections to other regions (e.g., LFG and LTG electrodes). A schematic of the electrodes in the IF and CF state is reported in Fig. 6 H and I, respectively.

Fig. 7 A and B depicts the AUC values for the IF and CF analysis in patient 4, respectively. Similar to patient 1, Fig. 7A shows that an IF state consistently occurs in all of the seizures shortly after the electrographic onset time. Unlike patient 1, however, there was no CF state in patient 4, as indicated by the lack of states with $AUC > 0.6$ (Fig. 7B). The absence of this state was a characteristic feature of all of the patients with complex partial seizures without generalization (see next section).

Fig. 7 C and D show the centroid and the connectivity matrix corresponding to the IF state, respectively. The LPT, LMT, and LAT electrodes were associated with the minimal entries in the centroid vector (LMT cover the clinically assigned seizure onset zone) and the focal channels 41 and 46 (which belong to the LMT grid; see Fig. 7F) were disconnected from the rest of the electrodes except for a few weak connections to the LPT electrodes. Although the lack of secondary generalization determined a less strong connectivity during seizures, we still noted interregional connections (e.g., LPF and LPS, LOF and LLF, LOF and LPS). The LAT and LMT electrodes were sparsely connected intraregionally and lacked of strong connections to other brain regions, whereas the LPT electrodes were mostly disconnected. Fig. 7E shows brain images of the left hemisphere

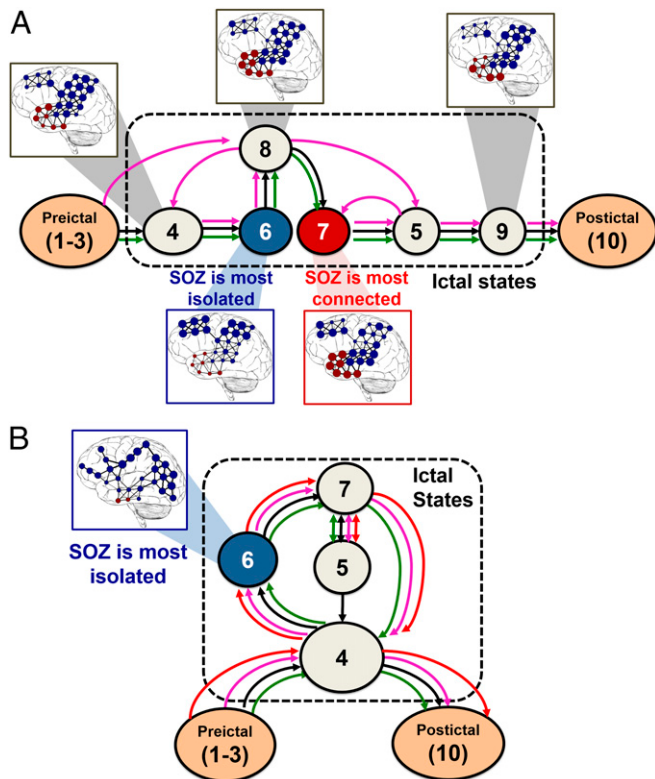


Fig. 5. (A and B) State transition diagrams corresponding to the states in Fig. 3H (A) and Fig. 4H (B), respectively. The networks are overlaid with brain images for a few states. Red nodes denote the annotated seizure onset zone and the diameter of each node is proportional to its EVC. Note that, in the IF states, the EVCs of the focal regions are small, which indicates a loss of connectivity from the rest of the network. In the CF state, instead, the EVC of the seizure onset zone is largest. SOZ, seizure onset zone.

and the inferior region with the arrangement of the electrodes and labeled resected areas. Fig. 7F shows a schematic of the IF state connectivity: the LPS and LPF electrodes were strongly connected (large dots), whereas the anterior part of LAT and inferior parts of LPT and LMT (i.e., the resected region) were disconnected.

Population Statistics. Fig. 8 shows the population results (i.e., 42 seizures from 12 patients). Patients were divided in three groups (Table 1): patients with secondarily generalized tonic-clonic seizures and a single resective surgery (group 1); patients with partial or complex partial seizures without generalization and with a single resective surgery (group 2); patients with partial seizures without generalization who received more than one resective surgery (group 3). To compare properties across seizures, each seizure was normalized to be of unit length. Fig. 8 D–F reports the results of the statistical tests on the response in these groups with the 90th, 95th, 99th, and 99.5th percentiles. Percentiles were derived nonparametrically by using a simulation-based shuffle method (*Materials and Methods*).

For group 1, high AUC values (i.e., $AUC > 0.7$; Fig. 8A) for the IF analysis are associated with the focal area being isolated, whereas low AUC values (i.e., $AUC < 0.3$) indicate that the focal area is strongly connected. All of the AUC curves had a stereotypical shape with high values at the onset time, a rise during the beginning of the seizure, a fall later in the seizure, and second rise (back to ~ 0.5) at the end of the seizure. The rising period occurred at a consistent time in all of the patients, whereas the timing of the

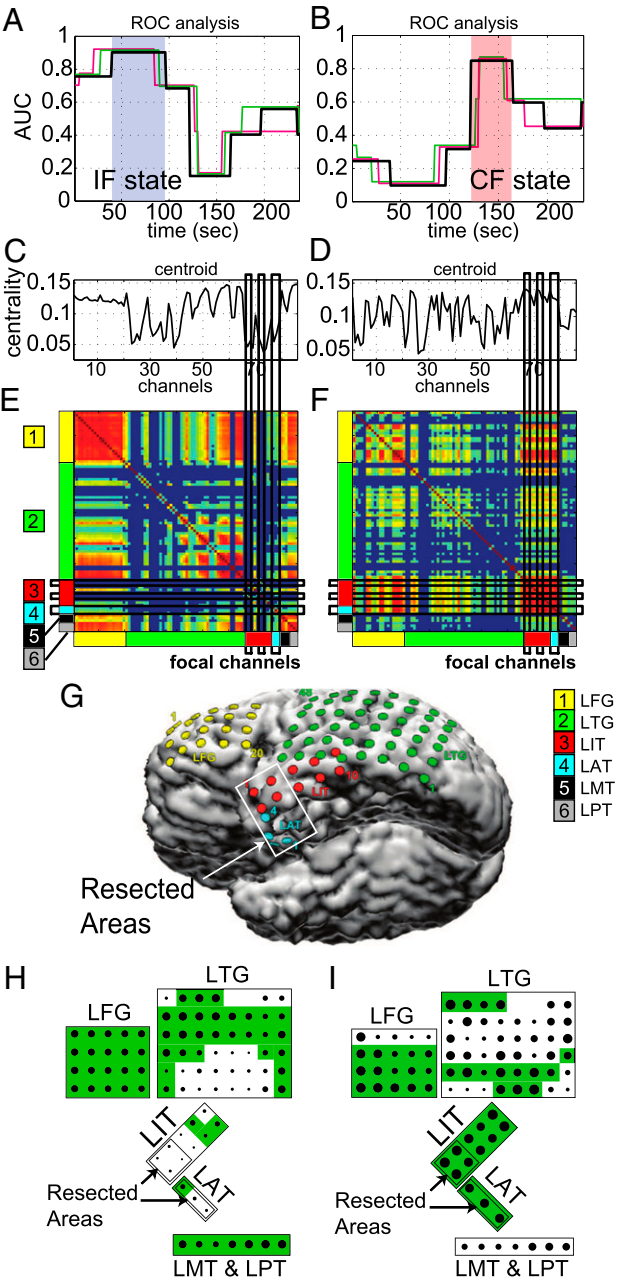


Fig. 6. Receiver operator characteristic (ROC) analysis for the patient in Fig. 3. (A and B) Area under the ROC curve (AUC) generated by comparing the resected areas to the inverted centroids (A) and to the centroids (B) corresponding to the states in Fig. 3H. Color code is as in Fig. 3H. The states corresponding to the IF and CF are shaded in blue and red, respectively. (C and D) EVCs of the IF centroid corresponding to the shaded state in A (C) and EVCs of the CF centroid corresponding to the shaded state in B (D). (E and F) Average connectivity matrix assigned to the IF state (E) and the CF state (F). The location of the electrodes in the brain is labeled on the axes. Channels in the matrix align vertically with the centroid in C and D, respectively. (G) Location of the electrodes on the brain. The resected area is in the white box. (H and I) Schematic of the dominant connectivity in the IF state (H) and in the CF state (I). The magnitude of the EVCs is indicated by the size of the dots, the connected regions are shaded green, and the resected areas are labeled.

drop was different across patients (hence, the drop was not in the mean value).

The period of high AUC values was statistical significant (above the 99.5th percentile; Fig. 8D) at the onset time and

during the first 40% of the seizure ($t=0.4$). This indicates that, during seizures with secondary tonic-clonic generalization, the seizure onset zone was significantly isolated from the remaining areas at the onset time and through the early stages of the seizures with the most isolated time occurring at $t=0.2$. Furthermore, we tested the significance of the AUC values for each patient in group 1 individually, and we found that the drops in AUCs were significant at the 99.5th percentile in two out of three patients ($t=0.9$ and $t=0.6$; red and magenta lines, respectively; Fig. 8A). This indicates that the seizure onset zone may be highly connected during late stages of the seizures, but, unlike the IF state, the timing of the CF state is not consistent across seizures.

For group 2, we noted more heterogeneous responses and, on average, larger peaks in the AUC value at the seizure onset time and smaller peaks around seizure termination (Fig. 8B). Individual patients had peaks that aligned with subsets of these population peaks. One patient (green line) showed no indication of IF, whereas another patient (orange line) had an IF for most of the seizure duration. Most of the patients, however, showed no period of low AUC values in case of IF analysis, which indicates that there was no time period when the seizure onset zone was strongly connected. The periods of high AUC values at onset and midseizure (i.e., $t \in [0.3 \text{--} 0.5]$) were both very significant (Fig. 8E), which means that, during partial seizures, the seizure onset zone is isolated from the rest of the areas at onset and midseizure.

For group 3 (i.e., patients with persistent postsurgery ictal activity, which required additional resective surgeries), we found that the AUC values were close to the chance level (0.5, Fig. 8C), perhaps because either part of the resected areas was not focal or there were additional focal areas that were not removed during the resection. In both cases, the resected areas were unlikely aligned with the seizure onset zone and the poorly predictive power of the AUC values represents a result of this misalignment. The statistical analysis, in fact, revealed that there were no time periods for patients in this group wherein the clinically assigned seizure onset zone was significantly isolated from the other areas of the brain (Fig. 8F).

Statistical tests analogous to those reported in Fig. 8 were repeated for the AUC values derived with the CF analysis. Results indicate that there were no time periods during seizure in any of the three groups when the seizure onset zone was significantly connected to the other brain areas. We also tested the progression of the state changes during the seizures for each patient, and we found that, in 6 out of 12 patients, the progression was statistically significant ($P < 0.05$, Table 2), which indicates that a subpopulation of patients had very consistent sets of brain states they progressed through during seizures. For the remaining six patients, the P value was around 0.5, which suggests that the brain state progressions during seizures in these patients were likely random.

Discussion

We have shown that the brain activity recorded through subdural ECoG and depth electrodes in 12 patients with DRE can be described by a small number of discrete connectivity states during interictal stages (2–5 states), ictal stages (2–11 states), and the pre/postictal epochs defined around the seizures (1–5 states). We also found that the brain transitions through a consistent progression of states during seizures, which suggests the existence of a characteristic pattern of information flow across the brain during seizures.

The fact that the brain only visits a small number of states suggests that, although the cerebral activity may be highly complex, there exists a low-dimensional dynamical space in which the brain commonly operates. This reduced state space of brain dynamics accounts for mutual interactions and network effects among different brain regions, and can be accessed through a network-based approach as proposed here. In particular, the

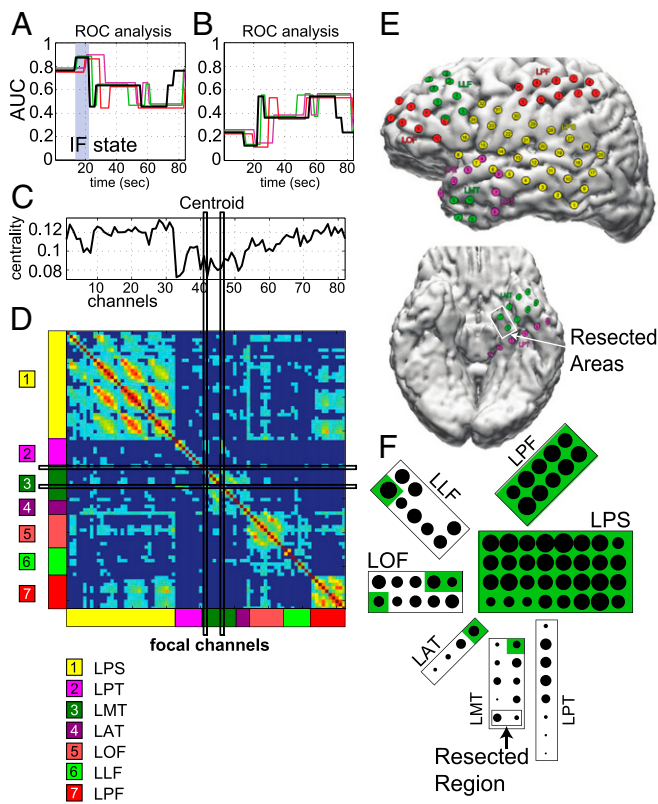


Fig. 7. ROC analysis for the patient in Fig. 4. (A and B) AUC values generated by comparing the resected areas to the inverted centroids (A) and to the centroids (B) corresponding to the states in Fig. 4H. Color code is as in Fig. 4H. The state corresponding to the IF is shaded in blue. Note that there is no CF state in any of the seizures in this patient. (C) EVCs of the IF centroid corresponding to the shaded state in A. (D) Average connectivity matrix assigned to the IF state. The location of the electrodes in the brain is labeled on the axes. Channels in the matrix align vertically with the centroid in C. (E) Location of the electrodes on the brain. Resected area is in the white box. (F) Schematic of the dominant connectivity in the IF state. The magnitude of the EVCs is indicated by the size of the dots, the connected regions are shaded green, and the resected areas are labeled.

existence of a finite set of states confirms that the transient neural activity of the brain has metastable properties (34, 35) and suggests that such activity changes during seizure events, whereas it is not apparently affected by cognitive processes or sleep/wake transitions (36). Moreover, because we uncovered these states by using ECoG recordings and we tracked the evolution of the brain network from one state to one another, our results suggest that a finite-state, data-driven model (e.g., hidden Markov model) could capture the brain dynamics, thus expanding the arrays of tools currently available to study brain activity and perform seizure onset time detection (37–40). Overall, these analyses could assist experts in identifying patterns that might not otherwise be readily evident.

Brain States and the Role of the Seizure Onset Zone. Recent evidence has indicated that the epileptic brain network may experience topological and functional alterations both during seizures and interictal stages, which can be captured by using network-based analyses (9, 11, 21, 26, 28, 35, 36, 41, 42). In particular, it has been shown both with local field potentials and ECoG recordings that during seizures the brain network evolves through a multifarious pattern of distinct topological structures, with the emergence of large subnetworks both at seizure onset and termination (9, 28). In contrast, during interictal stages, an increased

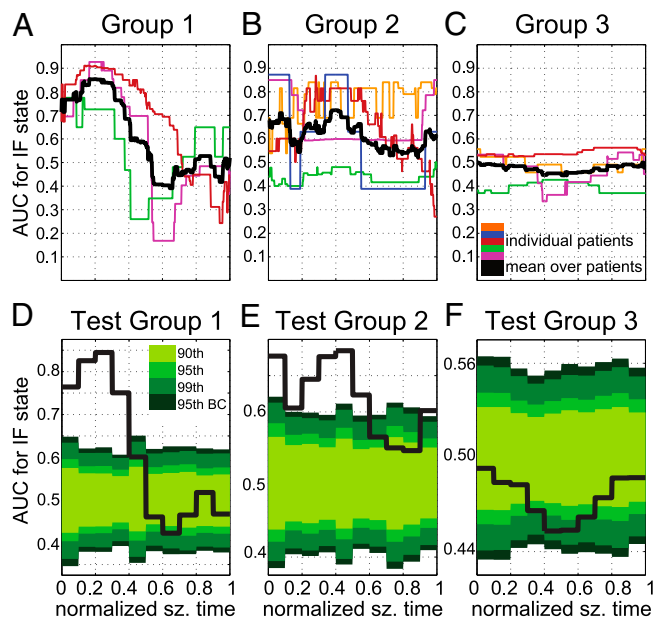


Fig. 8. Population-averaged results. (A–C) AUC values versus the normalized seizure time for the IF from patients in group 1 (A), group 2 (B), and group 3 (C), respectively. See Table 2. Color code in A–C: a black thick line indicates the average AUC value across the available patients in the group; nonblack lines indicate patient-specific AUC values (one line per patient). (D–F) Average AUC value from the plot in A (D), B (E), and C (F), respectively. Plots D–F are binned into 0.1 normalized time periods with simulation-derived percentiles in shades of green (from lightest to darkest: 90th, 95th, 99th, and Bonferroni corrected).

network regularity and the emergence of repetitive, metastable, frequency band-dependent scaffolds of brain connectivity has been reported (35, 36, 41).

Our approach provides further evidence to these observations and, in addition, it explores the temporal evolution of the brain network topology. In particular, we show that the emergence and recession of transient activity during interictal stages (35) actually corresponds to fluctuations between very few brain states (two to five states), which have similar levels of synchronization, are likely insensitive to cognitive conditions, and differ from the seizure-related states. Analogously, the multifarious topological progression of the brain network during seizures (9) inhabits only a small number of distinct states (Fig. 5), which capture the different levels of coalescence and fragmentation occurring in the brain network (36).

Furthermore, by combining postoperative follow-up information about the seizure onset zone (Table 1), we showed that the characteristic subnetwork topology emerging at seizure onset time (9, 11, 28) does not include the seizure onset zone, which remains significantly isolated from the remaining regions. This occurred across patients both with and without secondary generalization of the seizures (group 1 and 2), although the duration of the focal isolation was longer in seizures with generalization.

Interestingly, two out of three patients with secondary generalization of the seizures (group 1) also showed later stages during the seizure when the seizure onset zone was strongly connected to the rest of the recorded brain network ($P < 0.05$), even though these stages did not occur at the same time across patients and resulted in the mean not showing a connected time period (Fig. 3).

Based on the notion of centrality (30), the isolation of the seizure onset zone at the beginning of the ictal events is consistent with the fact that the seizure onset zone typically exhibits early abnormal ECoG activity compared with the remaining regions (6), which makes the connectivity of the seizure onset

zone to any other region in the brain relatively low. At later stages of the seizure, instead, the occurrence of strong hypersynchronization among different regions into an abnormal pattern determines an increase of the seizure onset zone's centrality, i.e., the seizure onset zone becomes highly connected in the network.

Interestingly, the difference between groups 1 and 2 could depend on how seizures propagate. Although purely speculative, it might be possible that, in the case of secondarily generalized seizures, the ictal activity might propagate more rapidly or has a larger focal region (43), and this would result in a shorter duration of the focal isolation. For patients who had partial seizures without secondary generalization and who had previous resective surgeries (group 3), instead, we could not consistently identify any time period with the seizure onset zone isolated or strongly connected. The lack of such periods could be a consequence of the misalignment between the resected areas and the seizure onset zone and/or inadequate electrode coverage of the brain. In particular, in patients who had previous resective surgeries, we analyzed ECoG recordings that were taken before the first resective surgery. The clinically reported resected areas included the whole set of regions resected across all of the surgeries to date. Hence, it is possible that, in these patients, the total resected area was larger than the clinically annotated seizure onset zone. This means that, when used with these recordings, our ROC-based resection indicator vector may have included electrodes that were not covering a focal region, and, therefore, it distorted the ROC analysis for these patients. Similarly, in patients who continued to experience seizures after all surgeries, the resected region may not include all of the seizure onset zone, and therefore our ROC-based resection indicator vector would have excluded electrodes that should have been included, again distorting our ROC analysis.

The strong difference between the results for groups 1 and 2 (single resective surgery) and group 3 (history of previous resective surgeries) suggests that our network analysis may be able to assist clinicians either in identifying a region of interest that likely contains the seizure onset zone or in suggesting that electrode coverage may not be adequate. Our ROC analysis on the EVC centroid values shows that the IF state identified in groups 1 and 2 reliably identifies the seizure onset zone. This suggests that, in cases where electrode coverage is likely adequate (as in groups 1 and 2 who had a single resective surgery), there should be a group of electrodes that disconnect from the brain network around the time of seizure onset. Therefore, one can compute the EVC during seizure events from the ECoG recordings and identify the group of electrodes (if any) that disconnects from the network around the time of seizure onset. If such a group is detected, then these regions can be identified as a "region of interest" for clinicians to carefully analyze. If no electrode disconnects from the network around the time of seizure onset, then clinicians can be informed that the "region of interest" is the empty set and reconsider the electrode coverage hypothesis.

Materials and Methods

Data Acquisition, Resection, and Postsurgical Outcome. Patients included in this study were surgically treated for drug-resistant seizures at the Johns Hopkins Hospital and underwent invasive presurgical monitoring with subdural grid-and-strip arrays for seizure localization or mapping of eloquent areas (Table 1). Clinical monitoring lasted five to seven days per patient and included two to seven clinical seizures. Decisions regarding the need for invasive monitoring and the placement of electrode arrays were made independently of this work and solely based on clinical necessity. The research protocol was reviewed by the Institutional Review Board (IRB) at The Johns Hopkins Hospital, and ECoG recordings were acquired without interfering with the clinical procedures and length of patient's stay after that informed consent was obtained.

Subdural grid arrays, strips, and depth-electrode arrays were implanted in various combinations as determined by clinical assessment for patients with

temporal, occipital, or frontal lobe seizures. Subdural grids had 20–64 contacts per array and were used in combination with subdural strips (four to eight contacts) or depth arrays, thus having 80–120 electrodes per patient over all. Intracranial contact locations were documented by postoperative CT coregistration with preoperative MRI.

The average length of the recording from each electrode in this study is 130.8 ± 40.9 h per patient (mean \pm SD). Recordings were acquired with a Stellate system (Stellate Systems) with 1,000-Hz sampling rate and 300-Hz antialiasing filter, and were converted to EDF format for storage and further processing. Each EDF file stored ~42 min of continuous ECoG data from all of the channels and it was automatically generated by the acquisition system. Consecutive EDF files cover consecutive, nonoverlapping time windows with less than 5-s lag in between. Digitized data were stored in an IRB-approved database compliant with Health Insurance Portability and Accountability Act (HIPAA) regulations.

Board-certified electroencephalographers (up to three) marked, by consensus, the unequivocal electrographic onset of each seizure and the period between seizure onset and termination. The seizure onset was indicated by a variety of stereotypical electrographic features, which include, but were not limited to, the onset of fast rhythmic activity, an isolated spike or spike and wave complex followed by rhythmic activity, or an electrodecremental response (6). Concurrently with the examination of the ECoG recordings, changes in the patient's behavior were sought from the video segment of video-ECoG recordings.

For each patient, we combined surgical notes about the electrodes corresponding to resected regions and postoperative follow-up information about how the resection affected the patient's seizures (Table 1). If, after surgery, a patient reported no seizures or could manage epilepsy with medications, then the resected areas were determined to correspond to the seizure onset zone. If the patient continued to have seizures after the resection, the resected region was determined to be smaller than or outside of the focal region. Finally, if the patient required multiple resections, the resected areas were determined to be larger than the seizure onset zone.

Spectral Analysis. The ECoG signals were processed in the referential recording configuration (i.e., each signal was referred to a common reference) and signals not related to the subdural activity (less than five signals per patient, e.g., signals from reference electrode, ECG electrode, etc.) were discarded. Because our analysis was conducted off-line on multiday continuous recordings, short-duration artifacts in the data likely due to movements (e.g., yawning, shaking, head turning, etc.) were not removed as they would have little impact. No long-duration artifacts (e.g., due to electrodes disconnected for several minutes) were present in our dataset. The sets of electrodes actually included in this analysis are reported in Table 2.

Each ECoG signal was divided into consecutive 2.5-s-long windows (1.5-s overlap). Each window (2,500 samples) was zero-phase filtered with a notch filter (notch frequency: 60 Hz; bandwidth: 4 Hz) and normalized by removing the mean and dividing by the SD. Then, the power spectrum of the window was estimated with the Welch's method (1-s-long segments, 75% overlap), thus resulting into a 1-Hz resolution (33).

The spectra over these windows were averaged separately over interictal and ictal periods and the ratio $R \triangleq \hat{P}_s / \hat{P}_i$ (r-spectrum) between the resulting average ictal and interictal spectra (\hat{P}_s and \hat{P}_i , respectively) was computed. For each patient, we evaluated the average r-spectrum in the frequency bands [1, 4] Hz, [5, 8] Hz, [9, 13] Hz, [14, 25] Hz, [25, 90] Hz, and [100, 200] Hz, and we selected the band where the maximum r-spectrum was achieved (Fig. 1).

Network Analysis. For each patient, the electrodes were treated as nodes in a graph and the strength of the edge between any two nodes was given by the average coherence between the ECoG recordings from those two electrodes in the band with maximum r-spectrum. For each patient, we used the following procedure:

- We divided the ECoG recordings into consecutive 3-s-long windows (2-s overlap) and, for each window $k = 1, 2, 3, \dots$, we computed the matrix $C(k)$, whose generic (i, j) th element is the coherence between the ECoG recordings of the i th and j th electrode in that window:

$$C_{ij}(k) \triangleq \frac{|P_{ij}(k)|^2}{P_{ii}(k) P_{jj}(k)}, \quad [1]$$

where $P_{ij}(k)$ is the cross-spectrum density between the i th and j th electrode averaged over the band with maximum r-spectrum in the window k , and $P_{ii}(k)$ and $P_{jj}(k)$ are the autospectrum densities for the i th and j th

electrode averaged over the same band, respectively. These spectra were computed with the Welch's method (1-s-long segments, 50% overlap). Note that the matrix $C(k)$ describes the topology of the graph in the window k ;

- ii)* To highlight the connectivity associated with the seizures, we computed the deviation $\hat{C}(k)$ of each matrix $C(k)$ from the average baseline connectivity, i.e., the generic (i, j) th element of $\hat{C}(k)$ was the element $C_{ij}(k)$ in Eq. 1 subtracted by the mean μ_{ij} and divided by the SD σ_{ij} of the elements C_{ij} over the entire interictal period. Furthermore, we retained the interpretation of the connectivity matrix as containing weighted connections on [0, 1] by using the transformation:

$$\bar{C}(k) \triangleq \frac{e^{\hat{C}(k)}}{1 + e^{\hat{C}(k)}}; \quad [2]$$

- iii)* For each matrix $\bar{C}(k)$, we computed the network EVC (30). Briefly, the centrality is a measure of how connected electrodes are in the network, i.e., an electrode has high centrality if it is strongly connected (high coherence) to many other electrodes. The EVC is measured by the leading eigenvector of $\bar{C}(k)$, i.e.:

$$EVC_k(i) = \frac{1}{\lambda(k)} \sum_j \bar{C}_{i,j}(k) \cdot EVC_k(j), \quad [3]$$

where $\lambda(k)$ is the leading eigenvalue of $\bar{C}(k)$ and EVC_k is the unit-length leading eigenvector of $\bar{C}(k)$. In this way, the i th element of EVC_k is a measure of the centrality of the i th electrode in the network (30). The leading eigenvector indicates a direction in the brain's state space and can be used to diagnose subspaces (network topologies) that correspond to different clinical states. For example, when the state of connectivity changes, the electrode centralities change, thus causing a rotation of the leading eigenvector. When the brain is consistently in a single state, instead, the leading eigenvector will only undergo small changes in direction.

Clustering of EVCs. The EVCs computed with Eq. 3 for each second $k = 1, 2, 3, \dots$, were separately clustered for the interictal periods, ictal periods, and for the preictal and postictal epochs (10 min before seizure onset and after seizure termination, respectively) by using a K-means algorithm with nonrandom centroid seeds (31). The duration of the pre/postictal epochs was chosen based on the patients' state evolution. Changes in the duration of these epochs (range: 5–15 min) did not alter our results significantly.

For any given number K of clusters, the nonrandom centroid seeds were determined as follows: *(i)* First, we computed the distance between the L_1 -norm of successive EVC vectors in time (L_1 -difference); *(ii)* then, we run the K-means algorithm and allocated the EVCs into K clusters; *(iii)* finally, we counted how many points in time were associated with a transition of the EVCs from one cluster to one another and the L_1 -difference exceeded a fixed threshold.

Steps *ii* and *iii* were repeated by lowering the threshold on the L_1 -difference until $K - 1$ time points exceeded the threshold. In this way, the time points exceeding this threshold correspond to the $K - 1$ times when the brain state was changing most rapidly. Then, we generated the K centroid seeds by averaging the EVCs between the maximum derivative time points from the beginning to the end of the record.

The actual number K of clusters was determined by using the Gap statistics (32), a nonparametric method that compares the intracluster distance between clustered data points to the distances measured in observation-based simulated data.

1. Berg AT, Kelly MM (2006) Defining intractability: Comparisons among published definitions. *Epilepsia* 47(2):431–436.
2. Kwan P, et al. (2010) Definition of drug resistant epilepsy: Consensus proposal by the ad hoc Task Force of the ILAE Commission on Therapeutic Strategies. *Epilepsia* 51(6):1069–1077.
3. Ngugi AK, Bottomley C, Kleinschmidt I, Sander JW, Newton CR (2010) Estimation of the burden of active and life-time epilepsy: A meta-analytic approach. *Epilepsia* 51(5):883–890.
4. Engel J, Jr (1994) Epilepsy surgery. *Curr Opin Neurol* 7(2):140–147.
5. Spencer SS (2002) When should temporal-lobe epilepsy be treated surgically? *Lancet Neurology* 1(6):375–382.
6. Niedermeyer E, Lopes da Silva FH (2005) *Electroencephalography: Basic Principles, Clinical Applications, and Related Fields* (Lippincott Williams & Wilkins, Philadelphia), 5th Ed.
7. Bulacio JC, et al. (2012) Long-term seizure outcome after resective surgery in patients evaluated with intracranial electrodes. *Epilepsia* 53(10):1722–1730.
8. Widdess-Walsh P, et al. (2007) Subdural electrode analysis in focal cortical dysplasia: Predictors of surgical outcome. *Neurology* 69(7):660–667.
9. Kramer MA, et al. (2010) Coalescence and fragmentation of cortical networks during focal seizures. *J Neurosci* 30(30):10076–10085.
10. Kramer MA, et al. (2012) Human seizures self-terminate across spatial scales via a critical transition. *Proc Natl Acad Sci USA* 109(51):21116–21121.
11. Kramer MA, Kolaczyk ED, Kirsch HE (2008) Emergent network topology at seizure onset in humans. *Epilepsia* 49(2-3):173–186.
12. Netoff TI, Schiff SJ (2002) Decreased neuronal synchronization during experimental seizures. *J Neurosci* 22(16):7297–7307.

13. Schiff SJ, Sauer T, Kumar R, Weinstein SL (2005) Neuronal spatiotemporal pattern discrimination: The dynamical evolution of seizures. *Neuroimage* 28(4):1043–1055.
14. Schindler K, et al. (2010) Peri-ictal correlation dynamics of high-frequency (80–200 Hz) intracranial EEG. *Epilepsy Res* 89(1):72–81.
15. Schindler KA, Bialonski S, Horstmann MT, Elger CE, Lehnertz K (2008) Evolving functional network properties and synchronizability during human epileptic seizures. *Chaos* 18(3):033119.
16. Wendling F, Bellanger JJ, Badier JM, Coatrieux JL (1996) Extraction of spatio-temporal signatures from depth EEG seizure signals based on objective matching in warped vectorial observations. *IEEE Trans Biomed Eng* 43(10):990–1000.
17. Wu L, Gotman J (1998) Segmentation and classification of EEG during epileptic seizures. *Electroencephalogr Clin Neurophysiol* 106(4):344–356.
18. Mormann F, et al. (2005) On the predictability of epileptic seizures. *Clin Neurophysiol* 116(3):569–587.
19. Schindler K, Leung H, Elger CE, Lehnertz K (2007) Assessing seizure dynamics by analysing the correlation structure of multichannel intracranial EEG. *Brain* 130(Pt 1):65–77.
20. Feldt Muldoon S, Soltesz I, Cossart R (2013) Spatially clustered neuronal assemblies comprise the microstructure of synchrony in chronically epileptic networks. *Proc Natl Acad Sci USA* 110(9):3567–3572.
21. Morgan RJ, Soltesz I (2008) Nonrandom connectivity of the epileptic dentate gyrus predicts a major role for neuronal hubs in seizures. *Proc Natl Acad Sci USA* 105(16):6179–6184.
22. Roopun AK, et al. (2010) A nonsynaptic mechanism underlying interictal discharges in human epileptic neocortex. *Proc Natl Acad Sci USA* 107(1):338–343.
23. Andrzejak RG, Chicharro D, Lehnertz K, Mormann F (2011) Using bivariate signal analysis to characterize the epileptic focus: The benefit of surrogates. *Phys Rev E Stat Nonlin Soft Matter Phys* 83(4 Pt 2):046203.
24. Burns SP, et al. (2012) A network analysis of the dynamics of seizure. *Conf Proc IEEE Eng Med Biol Soc* 2012:4684–4687.
25. Schevon CA, et al. (2007) Cortical abnormalities in epilepsy revealed by local EEG synchrony. *Neuroimage* 35(1):140–148.
26. Warren CP, et al. (2010) Synchrony in normal and focal epileptic brain: The seizure onset zone is functionally disconnected. *J Neurophysiol* 104(6):3530–3539.
27. Yaffe R, et al. (2012) Brain state evolution during seizure and under anesthesia: A network-based analysis of stereotaxic eeg activity in drug-resistant epilepsy patients. *Conf Proc IEEE Eng Med Biol Soc* 2012:5158–5161.
28. Zaveri HP, et al. (2009) Localization-related epilepsy exhibits significant connectivity away from the seizure-onset area. *Neuroreport* 20(9):891–895.
29. Burns SP, Santaniello S, Anderson WS, Sarma SV (2013) State dynamics of the epileptic brain. *Proceedings of 6th ASME Annual Dynamic Systems and Control Conference*, 10.1115/DSCC2013-3708.
30. Newman MEJ (2010) *Networks: An Introduction* (Oxford Univ Press, Oxford).
31. Hastie T, Tibshirani R, Friedman JH (2009) *The Elements of Statistical Learning: Data Mining, Inference, and Prediction* (Springer, New York), 2nd Ed.
32. Tibshirani R, Walther G, Hastie T (2001) Estimating the number of clusters in a data set via the gap statistic. *J R Stat Soc Series B Stat Methodol* 63(2):411–423.
33. Bendat JS, Piersol AG (1986) *Random Data: Analysis and Measurement Procedures* (Wiley, New York), 2nd Ed.
34. Fingelkurts AA, Fingelkurts AA (2004) Making complexity simpler: Multivariability and metastability in the brain. *Int J Neurosci* 114(7):843–862.
35. Kramer MA, et al. (2011) Emergence of persistent networks in long-term intracranial EEG recordings. *J Neurosci* 31(44):15757–15767.
36. Yaffe RB, et al. (2014) Physiology of functional and effective networks in epilepsy. *Clin Neurophysiol*, 10.1016/j.clinph.2014.09.009.
37. Santaniello S, Burns SP, Anderson WS, Sarma SV (2014) An optimal control approach to seizure detection in drug-resistant epilepsy. *A Systems Theoretic Approach to Systems and Synthetic Biology: Models and System Characterization*, eds Kulkarni VV, Stan G-B, Raman K (Springer, New York, NY), Vol 1, pp 153–178.
38. Santaniello S, et al. (2011) Quickest detection of drug-resistant seizures: An optimal control approach. *Epilepsy Behav* 22(Suppl 1):S49–S60.
39. Santaniello S, Sherman DL, Thakor NV, Eskandar EN, Sarma SV (2012) Optimal control-based Bayesian detection of clinical and behavioral state transitions. *IEEE Trans Neural Syst Rehabil Eng* 20(5):708–719.
40. Santaniello S, Sherman D, Mirski M, Thakor N, Sarma SV (2011) A Bayesian framework for analyzing iEEG data from a rat model of epilepsy. *Conf Proc IEEE Eng Med Biol Soc* 2011:1435–1438.
41. Horstmann MT, et al. (2010) State dependent properties of epileptic brain networks: Comparative graph-theoretical analyses of simultaneously recorded EEG and MEG. *Clin Neurophysiol* 121(2):172–185.
42. Prinz AA (2008) Understanding epilepsy through network modeling. *Proc Natl Acad Sci USA* 105(16):5953–5954.
43. Yoo JY, et al. (2014) Ictal spread of medial temporal lobe seizures with and without secondary generalization: An intracranial electroencephalography analysis. *Epilepsia* 55(2):289–295.
44. Golub GH, Van Loan CF (1996) *Matrix Computations* (Johns Hopkins Univ Press, Baltimore), 3rd Ed.